

1 **Development and performance of a high-resolution surface wave and storm surge forecast model: Application**
2 **to a large lake**

3 **Laura L. Swatridge¹, Ryan P. Mulligan¹, Leon Boegman¹, and Shiliang Shan^{1,2}**

4 ¹ Department of Civil Engineering, Queen's University, Kingston, ON, Canada, K7L 3N6.

5 ² Department of Physics and Space Science, Royal Military College of Canada, Kingston, ON, Canada,
6 K7K 7B4.

7 Correspondence to: Laura Swatridge (l.swatridge@queensu.ca)

8

9 **Key Points:**

- 10
- A real-time forecast model of wind-driven hydrodynamics in Lake Ontario is developed.
- 11
- Model performance compares well with observed data and other forecast models.
- 12
- Forecast lead time impacts the accuracy of wave height and storm surge predictions.

13 **Abstract**

14

15 ~~A~~An automated real-time forecast model of surface hydrodynamics in Lake Ontario (Coastlines-LO) was
16 developed to automatically predict storm surge and surface waves. The system uses a dynamically coupled
17 Delft3D – SWAN model with a structured grid to generate 48 h predictions for the lake that are updated
18 every 6 h. The lake surface is forced with meteorological data from the High Resolution Deterministic
19 Prediction System (HRDPS). The forecast model has been running since May 2021, capturing a wide
20 variety of storm conditions. Good agreement between observations and modelled results is achieved, with
21 root mean squared errors (RMSE) for water levels and waves under 0.02 m and 0.26 m, respectively. During
22 storm events, the magnitude and timing of storm surges are accurately predicted at 9 monitoring stations
23 (RMSE < 0.05 m), with model accuracy either improving or remaining consistent with decreasing forecast
24 length. Forecast significant wave heights agree with observed data (1-12% relative error for peak wave
25 heights) at 4 wave buoys in the lake. Coastlines-LO forecasts for storm surge prediction for two consecutive
26 storm events were compared to those from the Great Lakes Coastal Forecasting System (GLCFS) to further
27 evaluate model performance. Both systems achieved comparable results with average RMSEs of 0.02 m.
28 Coastlines-LO is an open-source wrapper code driven by open-data and has a relatively low computational
29 demand, compared to GLCFS, making this approach suitable for forecasting marine conditions in other
30 coastal regions.

31

32 **1 Introduction**

33

34 Coastal regions of large lakes can face hazardous conditions with costly consequences due to strong storm
35 events, where powerful winds generate large waves and storm surge (Danard, 2003; FEMA, 2014;
36 Gallagher et al., 2020). Waves during these events can cause erosion, overtopping, and run-up, with the
37 hazards being greater when the water level is elevated from storm surge. The intensity and frequency of
38 strong storm events is increasing in the Great Lakes region as a result of climate change, as tropical storms
39 are predicted to reach higher latitudes more often (Bender et al., 2010; Studholme et al., 2022). In addition,
40 the mean water levels in the Great Lakes are being impacted by climate change, with large seasonal
41 fluctuations in lake levels and record low and high water levels consistently occurring in recent years
42 (Gronewold and Rood, 2019). The combined impacts of these projections present a greater risk for
43 hazardous conditions in Great Lakes coastal regions, and developing better methods to understand and
44 model the physical processes occurring during storms is important to help mitigate the risk. (Chisholm et
45 al., 2021; Gronewold et al., 2013).

46
47 'Real-time forecasting' of lakes and coastal oceans can be achieved by applying numerical models to run
48 predictive simulations of future hydrodynamic conditions in real time. Water level, circulation, and
49 temperature simulations, using forecast models of large lakes and reservoirs, aid in water quality
50 management (Baracchini et al., 2020; Carey et al., 2021; Lin et al., 2022). Coastal hazard forecasting is also
51 being applied in numerous ocean regions, including the northern Gulf of Mexico where forecast systems of
52 water levels and waves predict hurricane impacts on various scales (Bilskie et al., 2022; Dietrich et al.,
53 2018; Paramygin et al., 2017). Similarly, Rey and Mulligan (2021) use a coupled Deflt3D–SWAN model
54 to forecast storm conditions in coastal North Carolina, investigating the influence of various atmospheric
55 forecast models on the results during hurricanes. Specific to lakes, the National Oceanic and Atmospheric
56 Administration (NOAA) has implemented forecast models for North American coastal regions, including
57 the Great Lakes, with the Great Lakes Coastal Forecast System (GLCFS). The GLCFS uses a high-
58 resolution (30 m – 2 km) hydrodynamic model (FVCOM) to simulate physical processes including currents,
59 temperatures, and water levels (Kelley et al., 2018; Peng et al., 2019). Waves in the Great Lakes are
60 predicted by Environment and Climate Change Canada's (ECCC) Regional Ensemble Wave Prediction
61 System (REWPS), which uses a probabilistic approach to forecast wave characteristic 3 days into the
62 future.

63
64 Developing deterministic forecast models that run in real-time requires dealing with the challenge of
65 minimizing the computational runtime of the model while still achieving accurate results (model resolution
66 and performance), as the forecasts must be available in advance of the actual event. [This need to effectively
67 balance efficiency and accuracy in the real-time models is an active research area emphasized by \(Elko et
68 al., 2019\).](#) In addition, clear and efficient dissemination of forecasts must be provided to users and
69 stakeholders. Typical real-time coastal models require large computing resources to run high resolution
70 and accurate forecast simulations (Bilskie et al., 2022; Kelley et al., 2018), while fewer model applications
71 focus on developing flexible systems that can achieve accurate results while running on local computers,
72 often for smaller domains, using open data and with a smaller computational allowance (Lin et al., 2022;
73 Rey and Mulligan, 2021).

74
75 The accuracy of numerical models for simulating the hydrodynamic response of coastal regions to storm
76 events has increased with advances in computing power, data availability, and the development of models
77 that can better represent more physical processes and their interactions, however model performance is still
78 limited by the quality of input and forcing data available for a simulation. Model ability also depends on
79 the grid resolution, with higher resolution models being more capable of resolving bathymetric features

80 (Bilskie et al., 2022), and the inclusion of relevant processes, such as wave-current interactions and
81 baroclinic effects (Asher et al., 2019; Swatridge et al., 2022). A main consideration is the accuracy of the
82 atmospheric forcing, as winds are the primary driver of surface behaviour, and errors in the winds translate
83 through as errors in the modelled results (Dietrich et al., 2018; Farhadzadeh and Gangai, 2017; Rey and
84 Mulligan, 2021).

85
86 A probabilistic approach can be used to account for uncertainty in atmospheric forcing by running multiple
87 variations of the same event, however this requires large computational resources (Baracchini et al., 2020;
88 Fleming et al., 2008). In deterministic forecasts of water levels in Lake Erie, error in the atmospheric forcing
89 was significantly larger for 240 h forecasts compared to the 120 h forecasts, which translated to increased
90 error in predicted water levels (Lin et al., 2022). The longer forecast predicted excessive seiching and an
91 underestimation in peak water level, which improved as forecast length decreased. Forecasts of hurricane
92 storm surge and waves in the Gulf of Mexico by Forbes et al. (2010), Dietrich et al. (2018), and Bilskie et
93 al. (2022) found trends of decreasing error in storm surge prediction with shorter forecast length. Longer
94 forecasts (~5 days) resulted in storm surge variations of up to 4 m from the best track predictions, attributed
95 to variability in atmospheric forcing, and for forecasts shorter than 2.5 days, simulations converged on a
96 solution, and error was almost constant (Dietrich et al., 2018).

97
98 The hydrodynamics of Lake Ontario have been simulated on various scales in previous studies (e.g., Huang
99 et al., 2010; Paturi et al., 2012; Prakesh et al., 2007; Shore, 2009). Numerical models have also been used
100 to simulate waves and circulation during extreme events in the Kingston Basin (Cooper and Mulligan, 2016;
101 McCombs et al., 2014a; McCombs et al., 2014b). Sogut et al. (2019) used a combination of analyzing
102 historical water level and wave data, as well as numerical modelling of extreme storm events to gain insight
103 on lake seiching, storm surges, and wave patterns. Historical data have also been studied to determine the
104 risk of flooding due to storm surge along the Lake Ontario shoreline with a statistical model (Steinschneider,
105 2021). Surface waves and storm surge were simulated over the entire lake by Swatridge et al. (2022) during
106 recent storm events. Their study investigated the influence of different wind fields on the accuracy of storm
107 surge simulation, finding that variations in meteorological forcing were the primary source of uncertainty
108 in model results.

109
110 In the present study, an existing depth-averaged numerical model of Lake Ontario (Swatridge et al., 2022)
111 was applied to the lake to forecast water levels and waves in real-time, driven by spatially varied wind
112 fields from a high-resolution wind forecast model. The workflow develops an open-source Python- and
113 MATLAB-based wrapper code, that has been successfully applied to other systems using different

114 hydrodynamic models as part of the Canadian Coastal and Lake Forecasting Model System (Coastlines;
115 <https://coastlines.engineering.queensu.ca>; Lin et al., 2022; Rey and Mulligan, 2021). This flexible
116 methodology uses open access forcing/validation data and requires a relatively low computational demand,
117 compared to other existing Great Lakes storm surge models, allowing for application to other locations.
118 Model performance is evaluated by comparing results to near-real time observed data. Forecast results, for
119 storm surges and waves are statistically investigated over forecast lead times ranging from 6 to 48 h.

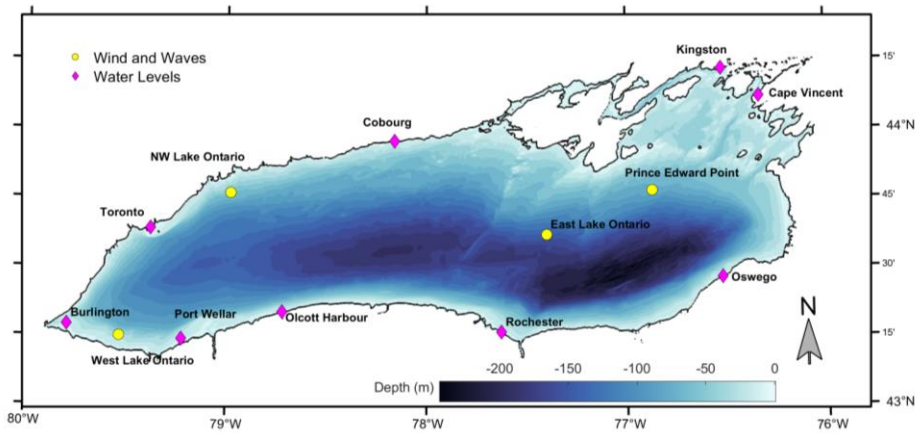
121 **2 Methods**

123 *2.1. Modelling Approach*

124 A two-dimensional (depth-averaged) coupled hydrodynamic-wave model is applied to Lake Ontario to
125 simulate wind driven hydrodynamics and waves using Delft3D-SWAN. The Delft3D flow model calculates
126 non-steady flow on a structured grid by solving the Reynolds-Averaged Navier Stokes equations (Lesser et
127 al., 2004). Wave conditions are simulated with the phase-averaged wave model, Simulating WAVes
128 Nearshore (SWAN), which uses the spectral action balance equation to compute random wind-generated
129 waves. SWAN accounts for non-linear wave interactions, wave propagation, refraction, dissipation due to
130 whitecapping, bottom friction and depth-induced breaking (Booij et al., 1999). The models are dynamically
131 coupled to account for wave-current interactions. Radiation stress gradients from SWAN simulations are
132 input into the horizontal momentum equations in Delft3D to account for the impacts of waves on
133 circulation, such as wave-induced mass fluxes driving currents, and enhanced bed shear stress. Results from
134 the hydrodynamic simulation are then used to update water levels and circulation in the wave model.

135
136 Model setup choices were made based on simulations by Swatridge et al. (2022) which were adapted for
137 the present study to minimize computational demand, allowing the system to run in real-time. The Delft3D
138 simulation uses a curvilinear grid with a horizontal resolution gradually ranging from 250-450 m. The wave
139 grid has a coarser resolution, ranging from 350-600 m, thus reducing the computational time required to
140 complete a wave simulation while still achieving higher resolution in nearshore areas ([Table S2 in the](#)
141 [supplementary material](#)). Flow simulations are depth-averaged and barotropic, shown by Swatridge et al.
142 (2022) to accurately represent surface storm surge in Lake Ontario, with root mean squared errors (RMSEs)
143 between observations and model results ranging between 0.01 m - 0.07 m during several major events.
144 Bathymetry data was interpolated to the grid from the US National Centers for Environmental Information's
145 (NCEI) 3-arcsecond (~ 90 m) resolution dataset with supplementary data from the ETOPO1 global relief
146 model with a resolution of approximately 1.3 km (Fig. 1). Detailed sensitivity testing for this model was
147 completed in Swatridge et al. (2022) to calibrate model parameters. Hydrodynamic simulations use a time

148 step of 120 s to satisfy the Courant–Friedrichs–Lewy stability criterion, and [coupling with the stationary](#)
149 [wave model occurs every 60 minutes, the wave model uses a stationary computational scheme. Coupling](#)
150 [between the flow and wave models occurs every 60 minutes.](#)



151 **Figure 1:** Map of Lake Ontario showing NCEI bathymetry and the location of real-time water level, wind,
152 and wave observation stations (Table 1, Table 2)

155 Spatially varied atmospheric input from the Meteorological Service of Canada (MSC) High Resolution
156 Deterministic Prediction System (HRDPS) is used to drive the model (Milbrandt et al., 2016). HRDPS is
157 an hourly assimilated forecast system downscaled from the larger scale Regional Deterministic Prediction
158 System (RDPS) that provides hourly predictions of surface pressure and wind velocity components with a
159 horizontal resolution of 2.5 km for the pan-Canada domain. The system runs every 6 h, predicting
160 atmospheric conditions 48 h into the future. This wind-forcing was successfully used by Swatridge et al.
161 (2022) to simulate the lake surface response to a range of storm conditions. Their modelled results for water
162 levels and surface waves agreed with observations at up to 16 locations in Lake Ontario, resulting in
163 maximum difference between predicted and observed peak wave heights and water levels of 0.4 m and
164 0.08 m, respectively. No lateral boundary conditions are applied to account for the influence of the riverine
165 flows (Niagara and St. Lawrence Rivers), as [results from previous modelling studies have concluded that](#)
166 [the hydrodynamic influence of river inflows and outflows is limited to within 10 km of the river mouth](#)
167 [and therefore can be neglected for simulations of lake wide water level over event based timescales](#)
168 [previous works have found the hydrodynamic influence of river flows is limited to within 10 km of the](#)
169 [river inlet, and therefore have a negligible impact on large scale circulation and water levels over event-](#)
170 [based timescales](#) (Prakash et al., 2007; McCombs et al. 2014a). [The closed based approach leads to](#)

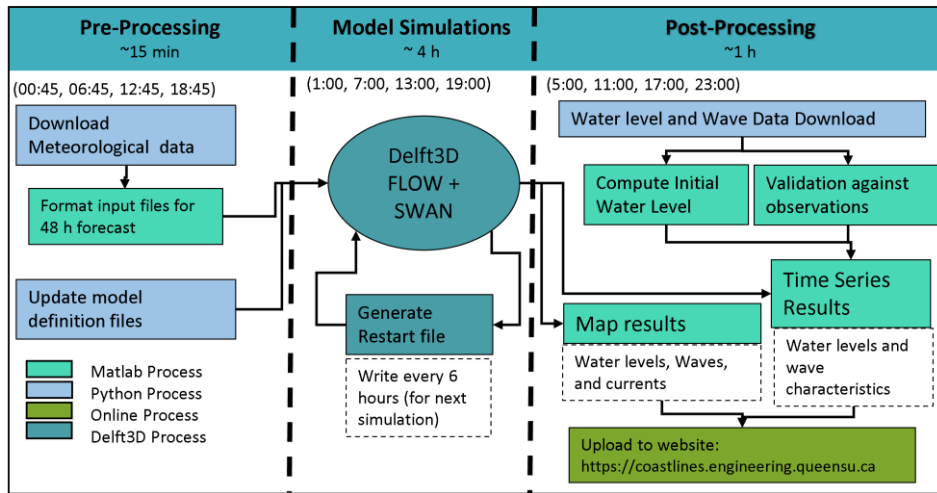
171 [uncertainties in the simulated results in the river region, however the impacts on the lake-wide hydraulics](#)
172 [is expected to be minimal.](#)

173

174 2.2. Development of an Automated Prediction System

175 The forecast system uses a combination of code written in MATLAB and Python to automatically run every
176 6 h and has been operational since May 2021 (<https://coastlines.engineering.queensu.ca/lake-ontario/>). The
177 workflow (Fig 2) consists of pre-processing, model simulation and post processing stages. For pre-
178 processing, initiation of the modelling system is scheduled to occur when a new HRDPS forecast becomes
179 available. Python is used to download the latest forecast and MATLAB is used to automatically process the
180 atmospheric forcing and write input files for Delft3D-SWAN. The Delft3D model definition files are then
181 updated with the correct time information.

182



183 **Figure 2.** Diagram of the automated workflow for processes performed for each model cycle (every 6 h
184 initiated by Windows Task Scheduler) on the local Coastlines server.

185

186 Model simulations cover a period of 48 h and are ‘hot-started’ with a restart file from a previous model run
187 if available. If a restart file is not available, simulations begin from rest with initial water levels of 0 m and
188 current speeds (u) of 0 m s^{-1} throughout the lake. When the simulation finishes, all available real-time
189 observed data, outlined in Table S1 in the supplementary material, is downloaded using Python, which is
190 then processed in MATLAB. Observed water levels at each station are averaged over the previous 12 h and
191 used to locally adjust the datum of the model outputs. We acknowledge that assimilating observed water

192 levels into the initial conditions may be a preferred approach, but this is beyond the scope of the present
193 study and may be incorporated into future versions on Coastlines-LO. The model simulates high frequency
194 variability in water levels generated by winds. Seasonal changes in water levels due to inflows, outflows,
195 and evaporation are not included, but are accounted for in post-processing.

196
197 Time series plots of observed water levels and wave heights are automatically compared to the forecast
198 model results from the previous 2.5 days at the observation locations and additional plots are created to
199 provide predictions at other locations of interest with no observed data (Fig. 1). Spatial snapshots of model
200 results across the lake are generated at select times, as well as animations showing key output parameters
201 during the forecast simulation. All outputs are exported to Google Sheets and displayed on the project
202 webpage, <https://coastlines.engineering.queensu.ca/>. The system runs in a Windows environment using 16
203 cores of a 32-core XEON workstation, with each workflow cycle taking approximately 5 h to complete a
204 48 h forecast simulation.

205

206 2.3. Real-time Comparison between Model Results and Observations

207 Near real-time observations of water surface elevation (η) data are available at 9 water level gauges around
208 the perimeter of Lake Ontario from the National Oceanic and Atmospheric Administration (NOAA) and
209 the Department of Fisheries and Oceans Canada (DFO), with temporal resolutions of 3 minutes and 6
210 minutes, respectively (Fig. 1; Table 1). Hourly surface waves and winds are measured in Lake Ontario at
211 one US National Data Buoy Center (NDBC) buoy and ECCO buoys from spring to early winter (Table 2).
212 The buoys report the significant wave height (H_s), peak wave period (T_p), surface wind speed and direction
213 averaged over an 8-minute period (U).

214

215 **Table 1:** List of real-time water level gauge station locations

<u>Name</u>	<u>Longitude</u>	<u>Latitude</u>	<u>Source</u>
<u>Oswego</u>	<u>-76.52</u>	<u>43.46</u>	<u>NOAA</u>
<u>Rochester</u>	<u>-77.63</u>	<u>43.27</u>	<u>NOAA</u>
<u>Olcott Harbour</u>	<u>-78.72</u>	<u>43.34</u>	<u>NOAA</u>
<u>Cape Vincent</u>	<u>-76.33</u>	<u>44.12</u>	<u>NOAA</u>
<u>Port Wellar</u>	<u>-79.22</u>	<u>43.24</u>	<u>DFO</u>
<u>Cobourg</u>	<u>-78.16</u>	<u>43.96</u>	<u>DFO</u>
<u>Burlington</u>	<u>-79.79</u>	<u>43.29</u>	<u>DFO</u>
<u>Kingston</u>	<u>-76.52</u>	<u>44.22</u>	<u>DFO</u>
<u>Toronto</u>	<u>-79.38</u>	<u>43.64</u>	<u>DFO</u>

216

217 **Table 2:** List of real-time wave buoy locations

Name	Longitude	Latitude	Depth	Source
Prince Edward Point	-76.87	43.78	68 m	ECCC
West Lake Ontario	-79.53	43.25	35 m	ECCC
Northwest Lake Ontario	-78.98	43.77	54 m	ECCC
East Lake Ontario	-77.40	43.62	140 m	NDBC

218

219 For long term analysis of results, the residual component of the water level data, representing storm surge,
 220 is isolated at the gauge locations by finding the difference between the total water level and the average
 221 water level, calculated using a gaussian window of 7 days (Steinschneider et al., 2021). Model performance
 222 is quantified using statistical measures including the RMSE (eq. 1), normalized RMSE (NRMSE; eq. 2),
 223 and the correlation coefficient (r; eq. 3):

$$224 \quad RMSE = \sqrt{\frac{\sum_{i=1}^n (x_i - y_i)^2}{n}} \quad (1)$$

$$225 \quad NRMSE = \frac{RMSE}{\bar{y}} \quad (2)$$

$$226 \quad r = \frac{\sum (y - \bar{y})(x - \bar{x})}{\sqrt{\sum (y - \bar{y})^2 \sum (x - \bar{x})^2}} \quad (3)$$

227 Where x_i and y_i ($i = 1, 2, 3, \dots, N$) are time series of modelled and observed data respectively, and N is the
 228 number of samples in the series. Strong storm surge events are identified from the water level data using
 229 the peaks-over-threshold method (Steinschneider et al. 2021). Forecast error during select events was
 230 evaluated by computing error metrics for consecutive forecasts leading up to the peak of the event. For each
 231 forecast, the relative error (RE; eq. 4), between observed and simulated maximum storm surge relative to
 232 the mean water level calculated at water level gauge locations, and between observed and modelled
 233 maximum wave heights at buoy locations was computed. The RMSE for each location was computed over
 234 a 6 h period that included the peak of the event.

$$235 \quad RE = \frac{|(\bar{y} - y) - (\bar{x} - x)|}{(\bar{y} - y)} \quad (4)$$

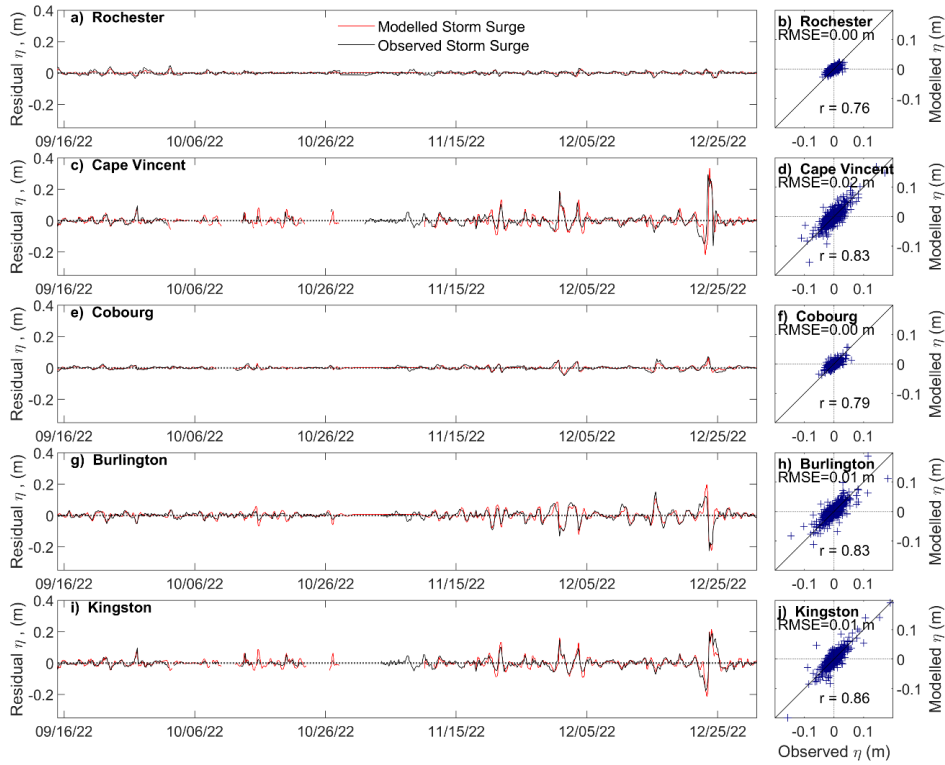
236

237 **3 Results**

238

239 *3.1. Long-term model performance*

240 Simulation results, for water levels and waves, at the observation locations, were compiled over the 20-
241 month operational period. The first 6 h of each 48 h forecast were stitched into a single time series, and
242 these results were compared to the observed data (Fig. S1 in the supplementary material). During this time,
243 seasonal changes in the observed mean lake level fluctuated by over 1 m, with the highest water levels
244 occurring in May 2022. The ability of the model to reproduce storm surge was investigated over a four-
245 month period when multiple storm events occurred (106 days from 15 September 2022 to 30 December
246 2022; Fig. 3). Stations with larger ranges of observed water levels (i.e., Burlington, Cape Vincent), located
247 at the east and west ends of the lake (i.e., Fig. 3c, g) show a slight bias, where the model tended to slightly
248 overpredict the maximum and minimum values, corresponding to larger RMSE values (Table 3). These
249 stations also tended to show a stronger correlation ($r = 0.83 - 0.86$); whereas observation points with
250 typically smaller ranges in water levels (Fig. 3a, e) resulted in weaker correlations ($r = 0.76 - 0.79$).
251 Normalized results show comparable error statistics at all stations, with larger errors occurring at locations
252 with smaller storm surges (i.e., Rochester, Oswego).
253



254
 255 **Figure 3:** Observed (black) and modelled (red) residual water levels at select observation points over a 3
 256 month period (September – December 2022) with corresponding scatter plots and error statistics over this
 257 period at select locations.
 258

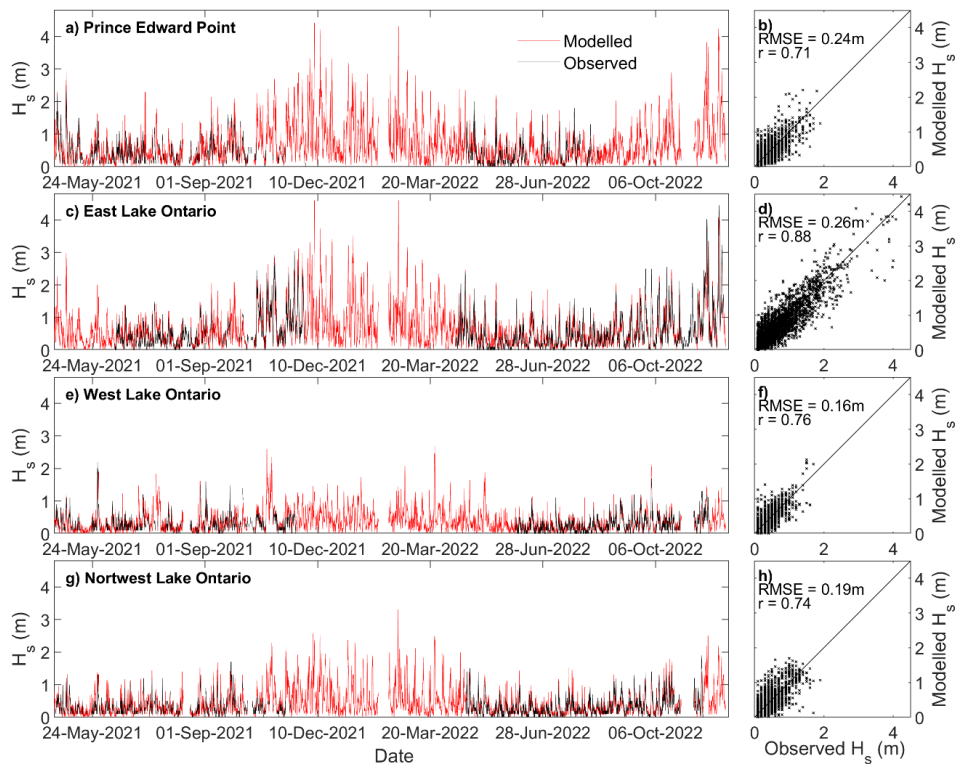
260 **Table 3:** Error Statistics for residual water level results over 106 days (September 15 – December 30, 2022)

	Minimum η (m)	Mean η (m)	Maximum η (m)	RMSE (m)	NRMSE (m)	r
Oswego	-0.10	0.07	0.12	0.01	0.15	0.80
Rochester	-0.03	0.03	0.04	0.00	0.16	0.76
Olcott	-0.16	0.04	0.11	0.01	0.19	0.80
Cape Vincent	-0.22	0.10	0.34	0.02	0.16	0.83
Port Wellar	-0.19	0.06	0.16	0.01	0.14	0.86
Cobourg	-0.08	0.04	0.07	0.01	0.14	0.79
Toronto	-0.16	0.07	0.14	0.01	0.14	0.83
Burlington	-0.22	0.10	0.20	0.02	0.14	0.83
Kingston	-0.21	0.09	0.25	0.01	0.14	0.86

261

262 Results for simulated H_s at buoy locations show the largest waves occurred during winter, between
 263 December and March (Fig.4). Results showing forecasted wave period compared to observations are shown
 264 in Fig S2 in the supplementary material. Over the 600-day operational period, no monitoring data was
 265 available for comparison and Lake Ontario could potentially experience partial ice-cover in nearshore areas,
 266 impacting the wave environment (Anderson et al., 2018). Stations in the eastern end of the lake (Prince
 267 Edward Point, East Lake Ontario) ~~are expected to experience the largest waves due to the experienced the~~
 268 ~~largest waves, due to the~~ prominent north-easterly direction of storms over the lake, ~~which results in winds~~
 269 ~~blowing along the long-axis of the lake creating a resulting in a larger~~ fetch at these locations (Lacke et al.
 270 2007; McCombs et al. 2014a). Error statistics show similar values for RMSE at these points however Prince
 271 Edward Point had the lowest correlation coefficient (Fig. 4a, b; $r = 0.71$), while East Lake Ontario showed
 272 the highest correlation (Fig. 4c, d; $r = 0.88$). Lower RMSE were at stations with smaller waves (Fig. 4e, g),
 273 and normalized results (Table 3) show comparable results at all buoys (NRMSE = 0.42 – 0.53 m).

274



275
 276 **Figure 4:** Time series of observed (black) and modelled (red) significant wave height over the duration that
 277 the buoys were in the lake (September -December 2022) with corresponding error scatter plots at the
 278 location of the 4 buoys. Note that the model was offline and are unavailable between February 9 – 27, 2022
 279 due to a change of service for the meteorological inputs.
 280

281 **Table 3:** Error statistics for significant wave heights at the buoy locations over 600 days (April 21, 2021 –
 282 December 12, 2022)

Location	Mean H_s (m)	Maximum H_s (m)	RMSE (m)	r	NRMSE (m)
Prince Edward Point	0.44	3.82	0.24	0.71	0.53
East Lake Ontario	0.62	4.42	0.26	0.88	0.42
West Lake Ontario	0.34	2.60	0.16	0.76	0.48
Northwest Lake Ontario	0.35	2.29	0.19	0.74	0.53

283

284 3.2. Storm event forecasts

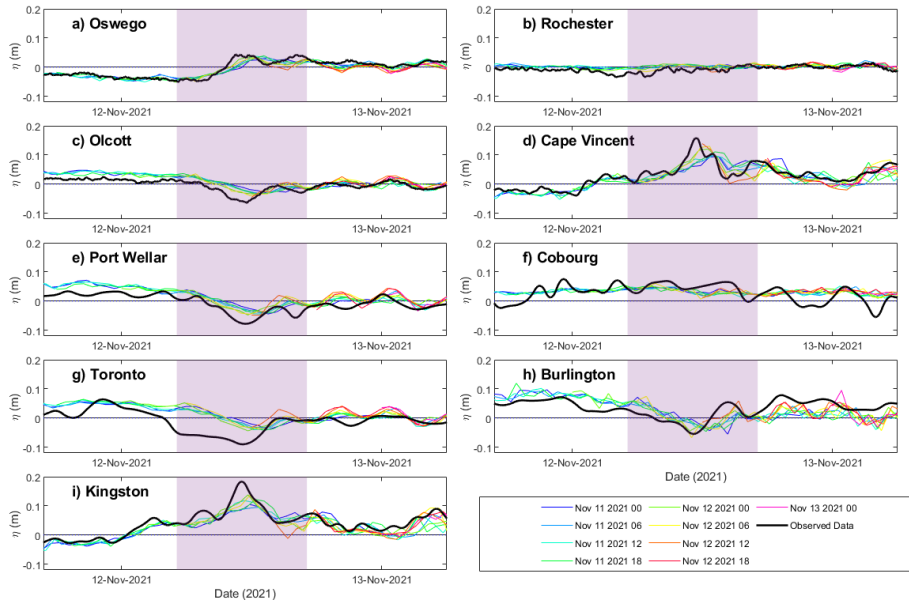
285 The performance of the model was evaluated over an event on November 12-12, 2021 consisting of wind
 286 speeds that approached 15 m s⁻¹, with the direction rotating clockwise from blowing towards the northeast
 287 to the winds dominantly blowing towards the east over a 24 h period. This event was selected due to the
 288 large storm surge generated ($\eta = 0.17$ m), and it resulted in the largest significant wave height that occurred
 289 over the 20 month operational period ~~in which~~ which generated the largest waves and storm surge over the
 290 20 month operational period with available observed water level and ~~with~~ wave measurements ~~data~~
 291 available from all buoy locations for comparison. ~~During this event, wind speeds reached up to 15 m s⁻¹,~~
 292 ~~with the direction rotating clockwise from the southeast to the west over a 24 h period.~~ Overlapping 48 h
 293 HRDPS forecasts (i.e., generated every 6 h) were validated against buoy observations, with good agreement
 294 found between modelled and predicted total wind speeds and directions, with peak wind speeds
 295 underrepresented by at most, 4.21 m s⁻¹ at Northwest Lake Ontario and overpredicted by up to 2.61 m s⁻¹ at
 296 Prince Edward Point (Fig. S3 in the supplementary material)

297

298 This event resulted in an observed storm surge of up to 0.16 m in the northeast region of the lake, at Cape
 299 Vincent and Kingston. The forecast simulations captured the timing and magnitude of the event peak, with
 300 predicted surge values ranging between 0.12 m – 0.17 m (Fig.5d, i). A set down of about 0.10 m was
 301 recorded at the Burlington station, which was underpredicted by the model by up to 0.05 m. The simulated
 302 results at this location predicted water levels up to 0.05 m higher than the observations for the 24 h preceding
 303 the storm (Fig.5h). Notable error can also be identified at Cobourg (Fig. 5f) with the model predicting
 304 negligible fluctuations in the water surface, but observations show some oscillations (0.05 m).

305

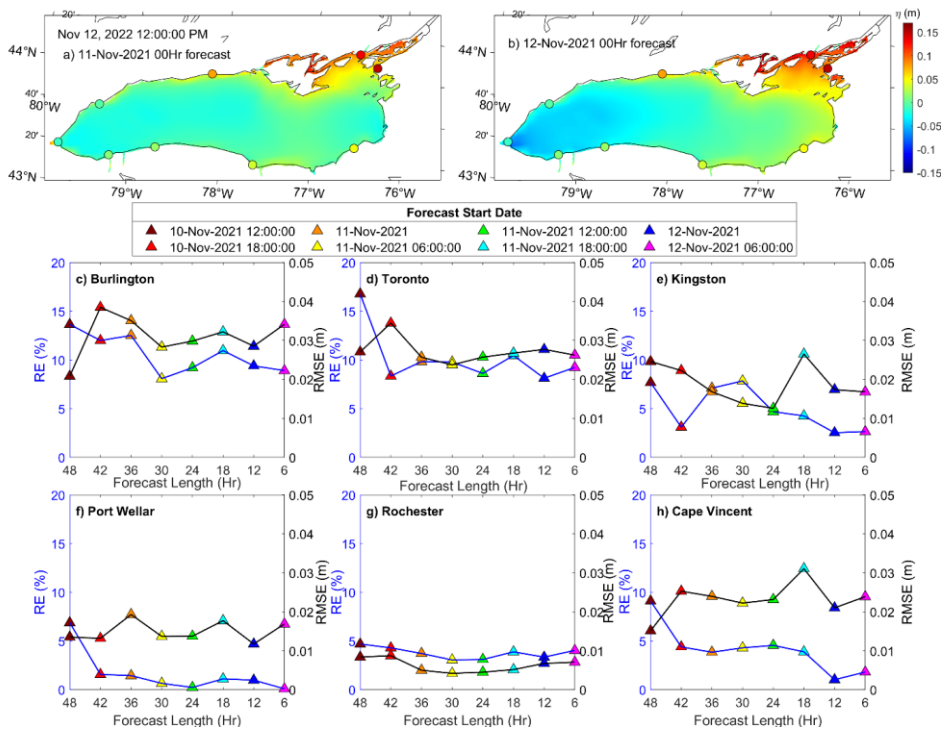
Formatted: Font: Italic



306
 307 **Figure 5:** Time series of measured water levels at various observation points compared to forecasted data
 308 from progressive model simulations. The highlighted area indicates the 12 h period over which error
 309 statistics are computed.

310
 311 Forecast performance was quantified by computing error statistics, over the duration of the event, for each
 312 forecast leading up to the time of peak water level. The largest errors occurred at the location of the set
 313 down, Burlington and Toronto, with a nearly constant RMSE of 0.03 m, and RE of 14% and 10%
 314 respectively (Fig. 6c, d). The errors at all stations remained fairly constant with RMSE and RE under 0.03 m
 315 and 10%, respectively, for each new forecast. However, map results showing the spatial variability in water
 316 level predictions from forecasts 12 h and 36 h before the storm peak show large differences (Fig. 6a,b). The
 317 earlier results (Fig. 6a) simulated a far less extensive storm surge in the northeast region of the lake than
 318 what was subsequently predicted 24 h later (Fig. 6b), when the storm surge was simulated to impact most
 319 of the northeast shoreline. The later forecast also predicted spatially larger set-down, about 0.10 m more
 320 than the earlier forecast in the western region of the lake.

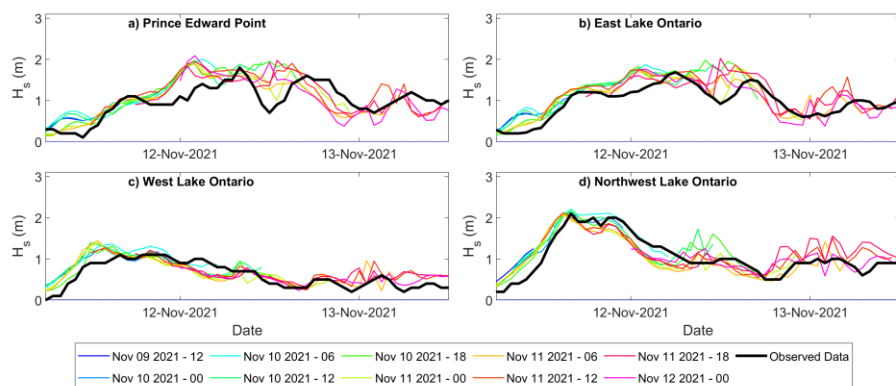
321



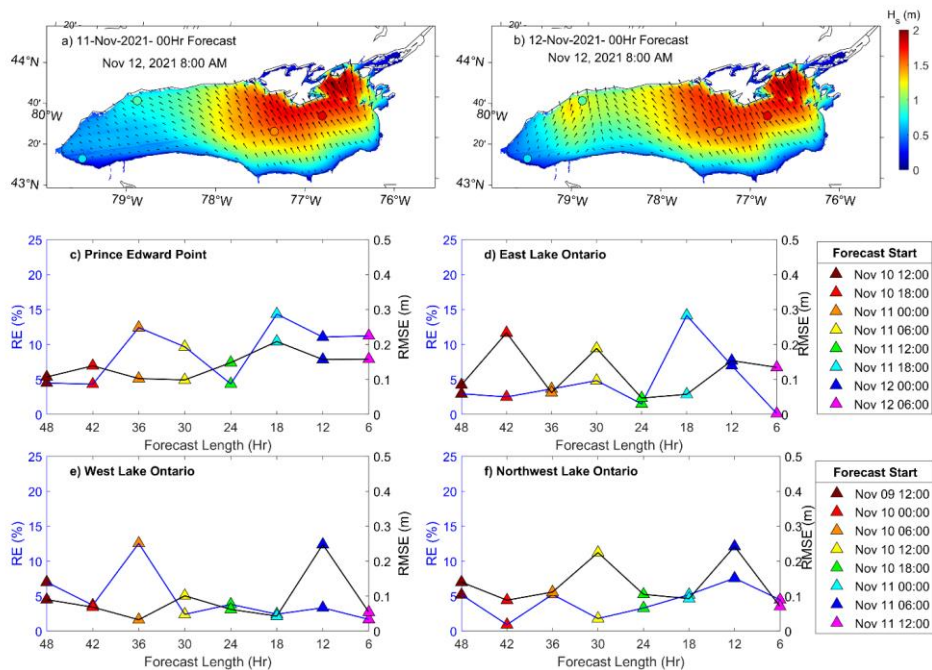
322
 323 **Figure 6:** Contour plots showing maps of modelled water levels at the peak of the storm event from two
 324 different forecasts, with an starting a) 35 hr lead time starting November 11, 00:00 UTC and b) 11 hour
 325 lead time starting on November 12, 00:00 UTC, with observed data plotted at the observation locations in
 326 black circles. Panels c) to h) show metrics including the RE and RMSE for peak storm surge magnitude at
 327 the locations of 6 selected water level gauges from the 8 forecasts preceding the storm event.

328
 329 Measured waves during this event reached up to 2.10 m, with the buoys in the western region of the lake
 330 (Fig. 7c, d) experiencing peak wave heights about 12 h earlier (Nov 11, 2021, 18:00 UTC) than the buoys
 331 in the eastern region of the lake (Fig. 7a, b, Nov 12 2021, 06:00 UTC). This is explained by the shift in
 332 wind direction over the storm duration, with winds originally from the southeast, rotating clockwise, then
 333 blowing dominantly from the west along the axis of the lake (Fig. S3 in the supplementary material).
 334 Overall, forecast simulations captured the magnitude of the waves all stations, with some error, and
 335 approximately 5 h delay in the timing of the peak H_s at Prince Edward Point (Fig. 7a). Error for waves
 336 during this event, at all stations, was constant for consecutive forecasts at all stations, with RMSE for

337 between 0.03 – 0.25 m and RE between 1-12%. Despite the generally consistent results, at the buoy
338 locations, maps from different forecasts show distinct changes between the 36 h forecast (Fig. 8a) and the
339 6 h forecast (Fig. 8b). Simulated wave fields in the northeast region of the lake showed similar results
340 between forecasts, but in the northwest, predicted wave magnitudes and directions were distinctly different.
341 The earlier forecast predicted waves under 0.70 m coming from the southeast, whereas the later forecast
342 showed larger waves ($H_s = 0.50 - 1.00$ m) from the southwest, which can be attributed to changes in
343 forecasted wind-fields.
344



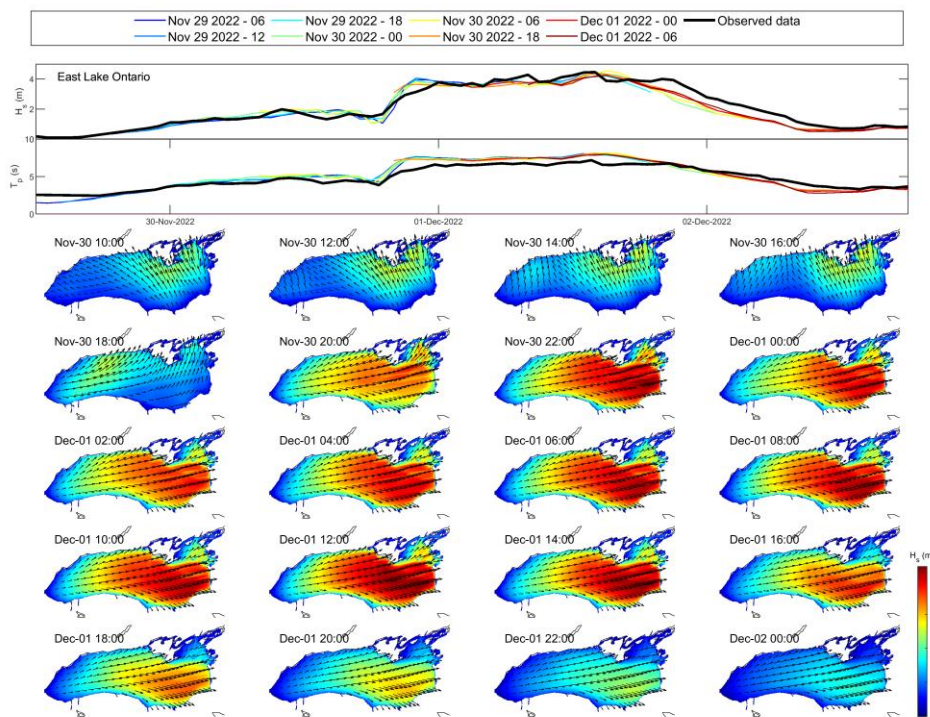
345
346 **Figure 7:** Time series of measured H_s at the location of the 4 buoys compared to modelled data from
347 progressive model forecasts for Event 1 (November 12, 2021).



348
 349 **Figure 8:** Contour maps of modelled waves with vectors indicating wave direction at a select time during
 350 the storm event, the peak of the storm event, from two forecasts, with: ~~an~~ a) 32 hr lead time starting starting
 351 ~~at~~ November 11, 00:00 UTC; and b) 8 hr lead time starting November 12, 00:00 UTC with observed data
 352 plotted at the observation locations in black circles. Every 10th vector is plotted for clarity. Panels c) to f)
 353 show metrics including the RE and RMSE for significant wave height at the locations of 4 buoys from the
 354 8 forecasts preceding the storm event on November 12, 2021, 12:00 UTC, and RMSE values are computed
 355 over a 12 h period centered at the time of the peak H_s for each station.

356
 357 For further investigation into model performance during storm events, wave forecasts during the event that
 358 resulted in the largest observed wave heights (December 1, 2022, Fig. 3c) were examined. During this
 359 storm, the lake experienced sustained easterly winds for almost 24 h, reaching speeds $> 20 \text{ m s}^{-1}$ on
 360 December 1, 14:00 UTC, generating waves $> 4 \text{ m}$ (Fig. 9). Data was only available from the one buoy at
 361 East Lake Ontario during this event, which recorded a maximum $H_s = 4.46 \text{ m}$. The forecasts initially
 362 underestimated this value, with a maximum predicted wave height of $H_s = 4.19 \text{ m}$ from the forecast starting
 363 on November 29 18:00 UTC, and the next forecast then overestimated this value ($H_s = 4.54 \text{ m}$). Subsequent

364 forecasts slightly underestimated the peak value, with the lowest predicted peak $H_s = 4.26$ m and the
 365 maximum values occurring ~ 1 h after the observed peak. All forecast results tended to overestimate the
 366 peak wave period, with predicted values ranging between 7.8 - 8.1 s, compared to an observed maximum
 367 value of 7.2 s.
 368

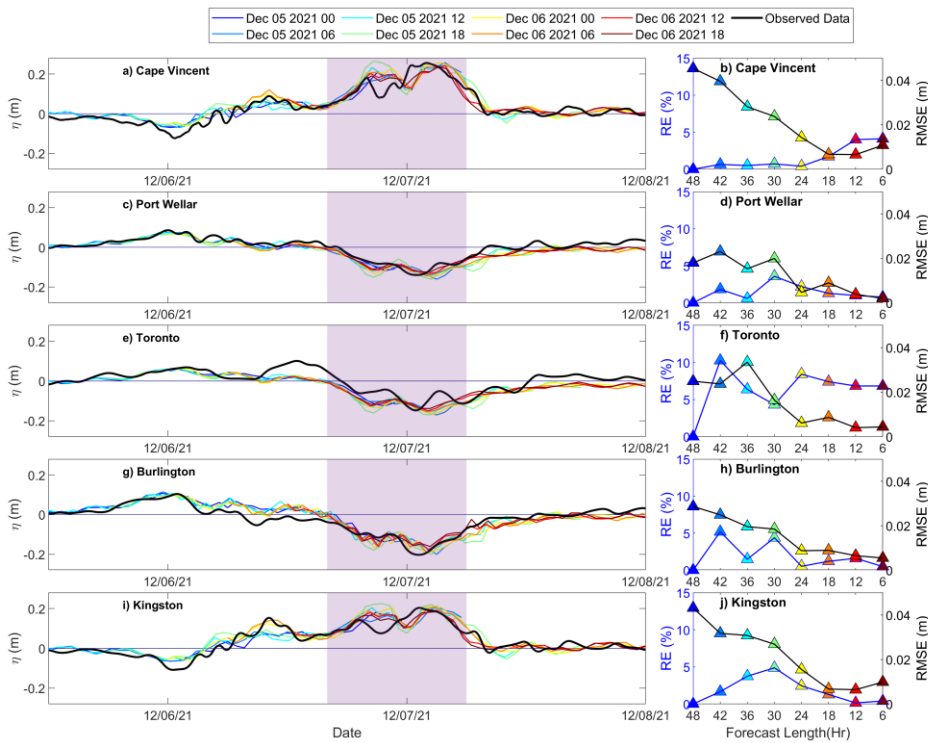


369
 370 **Figure 9:** Variability in significant wave height during a storm event: measured H_s compared to progressive
 371 forecast results at the Prince Edward Point Buoy for Event 3 (December 1, 2022; top) and maps of H_s and
 372 wave direction shown at an interval of 2 h (every 10th vector is shown for clarity).
 373

374 **4 Discussion**

375
 376 *4.1. Forecast Lead Times*

377 Water level forecasts during a storm event on December 8, 2021, were examined in relation to forecast lead
 378 time. During this event, 21 m s^{-1} winds (Figure S4 in the supplementary material) generated a storm surge
 379 of approximately 0.20 m along the northeast coast, and a resulting setdown of 0.10 m on the opposite end
 380 of the lake. Error statistics throughout the peak of the event, as a function of forecast lead time, were plotted
 381 at selected stations (Fig. 10). The timing and magnitude of the storm surge was well represented by the
 382 forecast model, with $\text{RMSE} < 0.05 \text{ m}$ for all forecasts and a maximum $\text{RE} = 14\%$.
 383



384 **Figure 10:** Time series of measured water levels at select observation points compared to forecasted data
 385 from progressive model simulations for Event 3: December 08, 2021, with corresponding plots showing
 386 computed RMSE calculated over the shaded area and percent error in peak storm surge from the 8 forecasts
 387 preceding the storm event.
 388

389
 390 Trends in the error can be identified for this event at all stations, with notable patterns corresponding to
 391 locations with larger fluctuations in water level (i.e., Cape Vincent, Kingston, Burlington). At these sites,

392 forecast error tended to decrease as the forecast length shortened. At Cape Vincent, the initial 48 h forecast
393 had an RMSE of 0.05 m and by the 18 h forecast, the RMSE had decreased to 0.01 m. However, after the
394 18 h forecast there was a slight increase in RE from less than 1% to about 5% (Fig. 10b). Trends in
395 decreasing error were also observed at Kingston, where a similar decrease in RMSE was observed, and the
396 RE was maintained between 1 – 5%, corresponding to a maximum underprediction of about 0.05 m (Fig.
397 10i, j). The locations with smaller ranges in surface fluctuations (Toronto, Port Wellar) generally showed
398 constant error (0.02 m and ~1% at Port Wellar; 0.01 m and 7% at Toronto) for consecutive forecast results
399 over the duration of this event (Fig. 10d, f).

400
401 Hydrodynamics in the model are only driven by atmospheric forcing, which is a primary source of
402 uncertainty in simulations of surface dynamics in large lakes. The accuracy of meteorological forecasts
403 typically decreases with increasing length due to assimilation schemes using observations and satellite
404 imagery to yield more accurate results (Buehner et al., 2015). Therefore, it is expected that hydrodynamic
405 forecast simulations will increase in accuracy as the lead time to a storm event decreases. For forecasts of
406 storm surges in other Great Lakes (e.g., Lake Erie; Lin et al., 2022) and coastal seas (e.g., Gulf of Mexico;
407 Dietrich et al., 2018), improvements in storm surge predictions are directly linked to increased accuracy in
408 meteorological forcing leading up to an event. However, our Lake Ontario model results do not follow a
409 consistent trend between different events, either improving (Fig. 10) or maintaining accuracy (Fig. 6;
410 Fig. 8). Cases where error increases (i.e., Fig 10b) or remains constant (i.e. Fig. 8), can be explained due to
411 sources of uncertainty in the model calibration and neglecting additional hydrodynamic processes in the
412 model setup (i.e. 3-dimensional circulation). Despite model accuracy being constant at the observation
413 locations, changes in the spatial variability of predicted water levels and wave conditions for different
414 forecasts are not clearly communicated through time series analysis but are qualitatively shown in maps of
415 results (Fig. 6; Fig. 10).

416

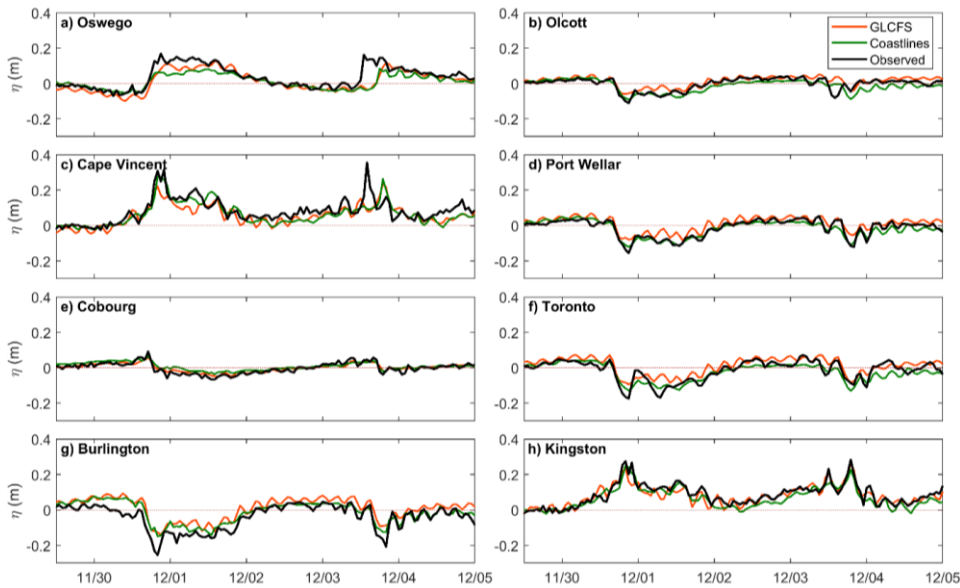
417 *4.2. Comparison with Other Models*

418 The current work (Coastlines-LO) makes use of a relatively simple, low computational demand modelling
419 approach. The performance of this model can be compared to the GLCFS, which delivers a higher resolution
420 and more complex forecast system in throughout the Great Lakes. Differences between predictions from
421 these models can be explained according to the setup of each system, including different hydrodynamic
422 models, grid resolutions, and atmospheric forcing inputs, which are summarized in table S23 in the
423 supplementary material. The GLCFS uses the 2 km horizontal resolution High Resolution Rapid Refresh
424 (HRRR) meteorological forcing, which is comparable to HRDPS (2.5 km), however previous studies have
425 found that wind and direction predictions can vary between these models (Rey and Mulligan, 2021;

426 Swatridge et al., 2022). The inclusion of waves in the two systems is also accounted for differently, with a
427 separate model (WaveWatch III) used to simulate waves in the GLCFS, while Coastlines-LO uses a
428 dynamically coupled wave and flow model that accounts for wave-current interactions. The inclusion of
429 wave coupling in simulations of the Great Lakes can impact water level predictions (Mao and Xia, 2017).
430 The GLCFS runs on NOAA's high performance computing system, and the larger computational power
431 allows it to include 3D baroclinic processes while still running in the required timeframe, whereas the
432 Coastlines-LO system in the present study uses a 2D, depth averaged approach, and therefore doesn't
433 resolve vertical gradients in lake temperature or 3D circulation. The inclusion of river inflows and outflows
434 in the GLCFS also allows the model to simulate seasonal changes in the mean lake water level instead of
435 accounting for these changes based on observed data in post-processing.

436
437 Forecasts results from both models were compared to observed data over a 6-day period in December 2022,
438 during which 2 storm events occurred (Fig. 11; Table S34 in the supplementary material). Results from the
439 first 6 h of subsequent forecasts are combined to construct a water level time series at observation points
440 for both models for the entire duration. Both models represent trends in water levels over this, resulting in
441 comparable metrics, with an average RMSE 0.02 m for both models, and $r = 0.73$ and 0.74 for Coastlines-
442 LO, and GLCFS, respectively. GLCFS achieved better predictions of peak water levels at Oswego for the
443 event on December 1 ($RE = 30\%$ for GLCFS, $RE = 51\%$ for Coastlines-LO; Fig. 11a), and more accurately
444 represented the surface fluctuations observed over the entire 6 day period at Toronto (Fig. 11f). While
445 GLCFS was able to represent water levels at some locations, Coastlines-LO had higher accuracy predictions
446 at others (Fig. 11c, d). At Port Wellar and Cape Vincent, Coastlines-LO better predicted the peak set-down
447 and set-up on December 1 by 0.01 m and 0.03 m respectively, while GLCFS underpredicted at these
448 locations by 0.05 m and 0.09 m. Both models had difficulty simulating the second storm surge (December
449 3) at Oswego and Cape Vincent (Fig. 11 a, c), where the observed surge occurs approximately 3 h before
450 the predicted peak. At the Kingston station (Fig. 11h), storm surges of 0.25 m and 0.30 m are observed.
451 Coastlines-LO yielded better predictions for the first event, simulating a peak value of 0.24 m, compared
452 to 0.28 m predicted by GLCFS, while GLCFS performed better for the second event, with a predicted storm
453 surges of 0.28 m and 0.22 m for GLCFS and Coastlines-LO, respectively. Therefore, while the GLCFS
454 offers several advantages, Coastlines-LO is able to provides comparable results for water level prediction
455 with a lower computational demand. This demonstrates that a relatively simple modelling system can be
456 applied to coastal environments to achieve accurate and efficient hydrodynamic predictions. The open-
457 source and flexible wrapper code could therefore be theoretically adapted. Coastlines-LO has the benefit of
458 a low computational demand and usage of the flexible open source wrapping code and that allows for easy
459 adaption to include different hydrodynamic models and investigate different field sites as previous works

460 have successfully applied similar approaches for forecast modelling (e.g., Lin et al., 2022; Rey and
461 Mulligan 2021), while still achieving very comparable results simulating short term water level
462 fluctuations in Lake Ontario.
463



464
465 **Figure 11:** Compiled Coastlines-LO forecast results compared to forecasts from the GLCFS and observed
466 data at select water level gauge locations interpolated to a 30 minute time resolution for 2 subsequent events
467 between November 30 – December 5, 2022.

468 4.3. Limitations and Uncertainties

469 Sensitivity testing and calibration of the numerical model this system is based on, comes from the work of
470 Swatridge et al. (2022), which found that 3D simulations of Lake Ontario improved predictions of surface
471 behaviour compared to 2D depth averaged simulations. The 3D simulation allowed the model to account
472 for transfer of surface momentum into baroclinic motions, giving a better representation of current
473 velocities and surface seiching following a storm event, resulting in reduced RMSE during storm events by
474 up to 12%, and improvement in modelled peak storm surge magnitude by up to 0.03 m. While 3D
475 simulations improved accuracy, they also increased the computational runtime of a 24 h simulation from
476 about 2.5 h to 4 h. Ten-day forecasts of 3D hydrodynamic processes in Lake Erie has been achieved by Lin
477 et al. (2022) in using the AEM3D model with a similar Coastlines computational workflow as the current
478 work; however, the Lake Erie model is on a coarser 2 km horizontal grid and does not couple with SWAN

479 to predict surface waves, which is computationally expensive compared to hydrodynamic simulations.
480 Therefore, to apply this model in real-time with a new simulation every 6 h, 2D simulations are used,
481 potentially resulting in up to 12% greater uncertainty in the forecast results. Additional investigation of
482 real-time model performance during more storm events, including when the lake is stratified is
483 recommended for further model validation.

484
485 There is additional uncertainty in model results during the winter season, when ice forms in the Great Lakes.
486 Lake Ontario typically experiences some ice cover between December and April (Anderson et al., 2018),
487 which impacts lake processes, including water levels, circulation, and waves through limited air-water
488 momentum transfer (Anderson et al., 2018; Farhadzadeh and Gangai, 2017). While ice cover has been
489 simulated in Lake Ontario using other models (e.g., Oveisy et al., 2012), it is presently not available in
490 Delft3D-SWAN. Therefore, simulations of surface behaviour during the ice-covered months would have
491 limited accuracy in ice-covered areas. Future work could incorporate ice cover into the model ~~by~~ applying
492 dynamic masking of ice-covered surfaces using satellite ~~data~~, to improve results during these months.

493
494 While this system requires low computational resources, making it flexible for adaption to other coastal
495 regions, it's capability for forecasting in additional locations is an area that requires future investigation. ~~making it possible to adapt it for other locations,~~ The applicability of the model is limited by the availability
496 of online data for model forcing and validation. In order to account for seasonal changes in mean lake
497 levels, near real-time measurements of water levels are needed in the simulation to adjust the datum in post-
498 processing. However, if no data were available the simulation could include the wind-generated short-term
499 fluctuations in surface levels and real-time operations could continue. The workflow of the model is also
500 limited by the availability of atmospheric forcing data, with any interruptions of service in the HRDPS
501 forecasts causing the hydrodynamic simulations to fail for that run-cycle. Improvements in the system could
502 account for this by providing a secondary source of atmospheric forcing in that case. In future studies, we
503 recommend applying this system to a region in the coastal ocean, therefore requiring the development of
504 real-time forecast inputs of open boundary conditions.

505
506

507 **5 Conclusions**

508

509 A forecast model for wind-driven hydrodynamics was developed and applied to Lake Ontario using an
510 approach with relatively low computational demand. Wind-waves and water levels were simulated using a
511 dynamically coupled Delft3D-SWAN model driven by high resolution atmospheric forcing. Simulations
512 were able to forecast the wind-driven variability in the lake surface, with seasonal changes in the total water

513 levels accounted for by adjusting the datum for each forecast cycle based on observations of the mean water
514 level. The system provides rapid (~5 h runtime) predictions that are publicly available through the project
515 webpage, with the automated system forecasting a 48 h period every 6 h. The model has been running
516 continuously since April 2021, capturing a variety of storm events with storm surges up to 0.30 m and
517 significant wave heights over 4.00 m. Reliable prediction for wave conditions during winter months are
518 provided by the forecast model when no wave observations are available, however accuracy is limited
519 where ice is present as this process is not included in the modelling system.

520

521 Results show that the model is effective in simulating short term fluctuations in the water levels and wave
522 conditions during strong storm events, with relative errors between observed and forecasted storm surge
523 magnitudes and significant wave heights of less than 15%. Larger errors typically corresponded to locations
524 in the lake with larger ranges in observed water levels. For storm events, as the forecast lead time decreases
525 for progressing forecasts, the simulated results changed as a result of updates to the meteorological forcing.
526 No constant trends in forecast error due to decreasing forecast length were apparent, with forecast accuracy
527 increasing with shorter forecasts in some cases and staying constant at others, but overall results agreed
528 well with observed data for all forecasts leading up to an event, with RMSE for storm surge and waves
529 below 0.05 m and 0.30 m, respectively. The model compared well with other existing forecast models in
530 the Great Lakes (GLCFS), yielding comparable results for water level predictions during multiple storm
531 events. Due to the low computational requirements and pan-Canadian coverage from the High Resolution
532 Deterministic Prediction System forecasts, this model could be adapted to other Canadian lakes and coastal
533 seas with available bathymetry data for storm surge prediction and monitoring.

534

535 **6 Code and Data Availability Statement**

536

537 Real-time model results are available at <https://coastlines.engineering.queensu.ca/lake-ontario/>, and
538 archived on the local server, to be made available by contacting the corresponding author. HRDPS input
539 data is available from the Meteorological Service of Canada Datamart and observed data is openly
540 accessible online, as cited in the text. The source code and documentation of the open source numerical
541 model (Delft3D 4.01.01) can be accessed on their online repositories
542 (<https://oss.deltares.nl/web/delft3d/source-code>, last access: 19 December, 2023). The Python and
543 MATLAB scripts, and supporting files used in the automated workflow, as well as data and scripts used
544 to generate the plots presented in this paper are archived on Zenodo
545 (<https://doi.org/10.5281/zenodo.10407863>, Swatridge, 2023).

546

547 **7 Author contributions**

548
549 The concept of the COASTLINES-LO workflow was designed by RM, LB, SS, and LS, and LS
550 implemented the idea. LS developed the performed the model simulations. All authors contributed to the
551 validation of the model and interpretation of the results. LS wrote the manuscript with contributions from
552 LB, SS, and RM.

553 **8 Acknowledgments**

554
555 Funding for this research was provided by Natural Sciences and Engineering Research Council of Canada
556 (NSERC) under the Discovery Grant program awarded to R.P. Mulligan (RGPIN/04043-2018), and a
557 Queen's Dean's Research Fund award to L. Boegman, R.P. Mulligan and S. Shan.

558

559 **9. References**

- 560 Anderson, E. J., Fujisaki-Manome, A., Kessler, J., Land, G.A., Chu, P.Y., Kelley, J.G.W., Chen, Y., and
561 Wang, J.: Ice Forecasting in the Next-Generation Great Lakes Operational Forecast System
562 (GLOFS). *J. Mar. Sci. Eng.*, 6(4), 123, <https://doi.org/10.3390/jmse6040123>, 2018.
- 563 Asher, T.G., Luettich, R.A., Fleming, J.G., and Blandton, B.O.: Low frequency water level correction in
564 storm surge models using data assimilation. *Ocean Modelling*, 144,
565 <https://doi.org/10.1016/j.ocemod.2019.101483>, 2019.
- 566 Baracchini, T., Wuest, A., and Bouffard, D.: Meteolakes: An operational online three-dimensional
567 forecasting platform for lake hydrodynamics. *Water Research*, 172.1-12,
568 <https://doi.org/10.1016/j.watres.2020.115529>, 2020.
- 569 Bender, M.A., Knutson, T.R., Tuleya, R.E., Sirutis, J.J., Vecchi, G.A., Garner, S.T. and Held, I.M.:
570 Modeled impact of anthropogenic warming on the frequency of intense Atlantic hurricanes.
571 *Science*, 327(5964), 454-458, DOI: 10.1126/science.1180568, 2010.
- 572 Bilskie, M.V., Asher, T.G., Miller, P.W., Fleming, J.G., Hagen, S.C. and Luettich Jr. , R.A.: Real-time
573 simulated storm surge predictions during Hurricane Michael (2018), *Wea. Forecasting*, 37, 1085–
574 1102, <https://doi.org/10.1175/WAF-D-21-0132.1>, 2022.
- 575 Buehner, M., McTaggart-Cowan, R., Beaulne, A., Charette, C., Garand, L., Heilliette, S., et al.:
576 Implementation of Deterministic Weather Forecasting Systems Based on Ensemble-Variational
577 Data-Assimilation at Environment Canada. Part 1: The Global System, *Mon. Wea. Rev.*, 143,
578 2532–2559, <https://doi.org/10.1175/MWR-D-14-00354.1>, 2015.

579 Boojj, N., Ris, R.C., and Holthuijsen, L.H.: A third-generation wave model for coastal regions: 1. Model
580 Description and validation. *Journal of Geophysical Research: Oceans*, 104(C4), 7649-7666,
581 <https://doi.org/10.1029/98JC02622>, 1999.

582 Carey, C.C., Woelmer, W.M., Lofton, M.E., Figueiredo, R.J., Bookout, B.J., Corrigan, R.S., et al.:
583 Advancing lake and reservoir water quality management with near-term iterative ecological
584 forecasting, *Inland Waters*, 12(1), 107-120, <https://doi.org/10.1080/20442041.2020.1816421>,
585 2022.

586 Chisholm, L., Talbot, T., Appleby, W., Tam, B., and Rong, R.: Projected change to air temperature, sea-
587 level rise, and storms for the Gulf of Main region in 2050, *Elem Sci Anth.* 9(1), 1-14,
588 <https://doi.org/10.1525/elementa.2021.00059>, 2021.

589 Cooper, A.H., and Mulligan, R.P.: Application of a Spectral Wave Model to assess Breakwater
590 Configurations at a small craft harbour on Lake Ontario, *J. Mar. Sci. Eng.*, 2016, 4(3), 46,
591 <https://doi.org/10.3390/jmse4030046>, 2016,

592 Danard, M., Munro, A., and Murty, T.: Storm surge hazard in Canada. *Natural Hazards*, 28, 407-434,
593 <https://doi.org/10.1023/A:1022990310410>, 2003.

594 Dietrich, J. C., Muhammad, M., Curcic, M., Fathi, A., Dawson, C. N., Chen, S. S., and Luettich Jr., A.:
595 Sensitivity of Storm Surge Prediction to Atmospheric Forcing during Hurricane Isaac, *J. Waterway,*
596 *Port, Coastal, and Ocean Eng.*, 144(1), [https://doi.org/10.1061/\(ASCE\)WW.1943-5460.0000419](https://doi.org/10.1061/(ASCE)WW.1943-5460.0000419),
597 2018.

598 [Elko, N., Dietrich, C., Cialone, M.A., Stockdon, H., Bilksie, M. W., Boyd, B., Charbonneau, B., Cox., D.,](#)
599 [Desback, K., Elgar, S., Lewis, A., Limber, P., Long, J., Massey, C., Mayo, T., McIntosh, K., Nadal-](#)
600 [Caraballo, N.C., Raubenheimer, B., Tomiczek, T., Wargula, A. E. \(2019\). Advancing the](#)
601 [understanding of storm processes and impacts. *Shore & Beach*, 87\(1\).](#)

602 Farhadzadeh, A., and Gangai, J.: Numerical Modelling of Coastal Storms for Ice-Free and Ice-Covered
603 Lake Erie, *J. of Coastal Research*, 33(6), 1383-1396, [https://doi.org/10.2112/JCOASTRES-D-16-](https://doi.org/10.2112/JCOASTRES-D-16-00101.1)
604 [00101.1](#), 2017.

605 FEMA: FEMA Great Lakes Coastal Guidelines, Appendix D.3 Update. FEMA, 2014.

606 Forbes, C., Luettich, R.A., Mattocks, C.A., and Westerink, J.J.: A retrospective evaluation of the storm
607 surge produced by Hurricane Gustav (2008): Forecast and hindcast results, *Wea. Forecasting*,
608 25(6), 1577-1602, <https://doi.org/10.1175/2010WAF2222416.1>, 2010.

609 Fleming, J.G., Fulcher, C.W., Luettich Jr., R.A., Estade, B.D., Allen, G., and Winer, H.S.: A real time storm
610 surge forecasting system using ADCIRC, *Proceedings of the International Conference on Estuarine*
611 *and Coastal Modeling*, [https://doi.org/10.1061/40990\(324\)48](https://doi.org/10.1061/40990(324)48), 2008.

612 Gallagher, G.W., Duncombe, R.K., and Steeves, T. M.: Establishing Climate Change Resilience in the
613 Great Lakes in Response to Flooding, *Journal of Science Policy & Governance*, 17(1),
614 <https://doi.org/10.38126/JSPG170105>, 2020.

615 Gronewold, A.D., and Rood, R.B.: Recent water level changes across Earth's largest lake system and
616 implications for future variability, *J. of Great Lakes Research*, 45(1), 1-3,
617 <https://doi.org/10.1016/j.jglr.2018.10.012>, 2019.

618 Gronewold, A.D., Fortin, V., Lofgren, B., Clites, A., Stow, C.A., and Quinn, F.: Coasts, water levels, and
619 climate change: A Great Lakes perspective, *Climate Change*, 120, 697-711,
620 <https://doi.org/10.1007/s10584-013-0840-2>, 2013.

621 Huang, A., Rao, Y.R., Lu, Y., and Zhao, J.: Hydrodynamic modelling of Lake Ontario: An intercomparison
622 of three models. *Journal of Geophysical Research: Oceans*, 115(C12), 1-16,
623 <https://doi.org/10.1029/2010JC006269>, 2010.

624 Kelley, J.G.W., Chen, Y., Anderson, E.J., Lang, G.A., and Xu, J.: Upgrade of NOS Lake Erie Operational
625 Forecast System (LEOFS) to FVCOM: Model Development and Hindcast Skill Assessment; NOS
626 CS 40, NOAA; NOAA Technical Memorandum, <http://doi.org/10.7289/V5/TM-NOS-CS-40>,
627 2018.

628 Lacke, M. C., Knox, J. A., Frye, J. D., Stewart, A. E., Durkee, J. D., Fuhrmann, C. M., & Dillingham, S.
629 M. (2007). A climatology of cold-season non convective wind events in the Great Lakes region.
630 *Journal of Climate*, 20(24), 6012-6022. <https://doi.org/10.1175/2007JCLI1750.1>

631 Lesser, G.R., Roelvink, J.A., and Stelling, G.S.: Development and validation of a three-dimensional
632 morphological model, *Coastal Engineering*, 51(8-9), 883-915,
633 <https://doi.org/10.1016/j.coastaleng.2004.07.014>, 2004.

634 Lin, S., Boegman, L., Shan, S., and Mulligan, R.P.: An automatic lake-model application using near real-
635 time data forcing: Development of an operational forecast workflow (COASTLINES) for Lake
636 Erie, *Geosci. Model Dev*, 15(3), 1331-1353, <https://doi.org/10.5194/gmd-15-1331-2022>, 2022.

637 McCombs, M.P., Mulligan, R.P., Boegman, L., and Rao, Y.R.: Modelling surface waves and wind-driven
638 circulation in eastern Lake Ontario during winter storms, *J. Great Lakes Res.*, 40(3), 130-142,
639 <https://doi.org/10.1016/j.jglr.2014.02.009>, 2014a.

640 McCombs, M.P., Mulligan, R.P., and Boegman, L.: Offshore wind farm impacts on surface waves and
641 circulation in Eastern Lake Ontario, *Coastal Engineering*, 93, 32-39,
642 <https://doi.org/10.1016/j.coastaleng.2014.08.001>, 2014b.

643 Mao, M., and Xia, M.: Dynamics of wave-current-surge interactions in Lake Michigan: A model
644 comparison, *Ocean Modelling*, 110, 1-20, <https://doi.org/10.1016/j.ocemod.2016.12.007>, 2007.

645 Milbrandt, J.A., Belair, S., Faucher, M., Vallee, M., Carrera, M.L., and Glazer, A.: The Pan-Canadian High
646 Resolution (2.5 km) Deterministic Prediction System, *Weather and Forecasting*, 31(6), 1791-1816,
647 <https://doi.org/10.1175/WAF-D-16-0035.1>, 2016.

648 Oveisy, A., Boegman, L., and Imberger, J.: Three-dimensional simulation of lake and ice dynamics during
649 winter, *Limnol Oceanogr*, 57(1), 43-57, <https://doi:10.4319/lo.2012.57.1.0043>, 2012.

650 Paramygin, V.A., Sheng, Y.P., and Davis, J.R.: Towards the development of an operational forecast system
651 for the Florida coast, *J. Mar. Sci. Eng.*, 5(1), <https://doi.org/10.3390/jmse5010008>, 2017.

652 Paturi, S., Boegman, L., and Rao, Y.R.: Hydrodynamics of eastern Lake Ontario and the upper St. Lawrence
653 River, *J. Great Lakes Res.*, 38(4), 194-204, <https://doi.org/10.1016/j.jglr.2011.09.008>, 2012.

654 Peng, M., Zhang, A., Anderson, E.J., Lang, G.A., Kelley, J.G.W., and Chen, Y.: Implementation of the
655 Lakes Michigan and Huron Operational Forecast System (LMHOFS) and the Nowcast/Forecast
656 Skill Assessment, NOAA technical report NOS CO-OPS, 2019.

657 Prakash, S., Atkinson, J.F., and Green, M.L.: A semi-Lagrangian study of circulation in Lake Ontario, *J.*
658 *Great Lakes Res.*, 33(4), 774-790,
659 [https://doi.org/10.3394/0380-1330\(2007\)33\[774:ASSOCA\]2.0.CO;2](https://doi.org/10.3394/0380-1330(2007)33[774:ASSOCA]2.0.CO;2), 2007.

660 Rey, A.J.M., and Mulligan, R.P.: Influence of hurricane wind field variability on real-time forecast
661 simulations of the coastal environment, *Journal of Geophysical Research: Oceans*, 126(1), 1-20,
662 <https://doi.org/10.1029/2020JC016489>, 2021.

663 Shore, J.A.: Modelling the circulation and exchange of the Kingston Basin and Lake Ontario with FVCOM,
664 *Ocean Modelling*, 30(2-3), 106-114, <https://doi.org/10.1016/j.ocemod.2009.06.007>, 2009.

665 Sogut, D.V., Jensen, R.E., and Farhadzadeh, A.: Characterizing Lake Ontario Marine Renewable Energy
666 Resources, *Marine Technology Society Journal*, 53(2), 21-38,
667 <https://doi.org/10.4031/MTSJ.53.2.3>, 2019.

668 Steinschneider, S.: A hierarchical Bayesian model of storm surge and total water levels across the Great
669 Lakes shoreline – Lake Ontario, *J. Great Lakes Res.* 47(3), 829-843,
670 <https://doi.org/10.1016/j.jglr.2021.03.007>, 2021.

671 Studholme, J., Fedorov, A.V., Gulev, S.K., Emanuel, K., and Hodges, K.: Poleward expansion of tropical
672 cyclone latitudes in warming climates, *Nature geoscience*, 15, 14-18,
673 <https://doi.org/10.1038/s41561-021-00859-1>, 2022.

674 Swatridge, L.L., Mulligan, R.P., Boegman, L., Shan, S., and Valipour, R.: Coupled modelling of storm
675 surge, circulation, and surface waves in a large, stratified lake, *J. Great Lakes Res*, 48(6), 1520-
676 1535, <https://doi.org/10.1016/j.jglr.2022.08.023>, 2022.